Coexistence of magnetic order and spin-glass-like phase in the pyrochlore antiferromagnet $Na_3Co(CO_3)_2Cl$

Zhendong Fu,[1,*] Yanzhen Zheng,[2,7,†] Yinguo Xiao,[3] Subhankar Bedanta,[4] Anatoliy Senyshyn,[5,6] Giovanna Giulia Simeoni,[5] Yixi Su,[1] Ulrich Rücker,[3] Paul Kögerler,[3,7] and Thomas Brückel[3,‡]

[1]*Jülich Centre for Neutron Science JCNS, Forschungszentrum Jülich GmbH, Outstation at FRM II, Lichtenbergstraße 1, D-85747 Garching b. München, Germany*

[2]*Center for Applied Chemical Research, Frontier Institute of Science and Technology, Xi'an Jiaotong University, 710049 Xi'an, China*

[3]*Jülich Centre for Neutron Science JCNS, Peter Grünberg Institut PGI, JARA-FIT, Forschungszentrum Jülich GmbH, D-52425 Jülich, Germany*

[4]*School of Physical Sciences, National Institute of Science Education and Research, 751005 Orissa, India*

[5]*Forschungsneutronenquelle Heinz-Maier Leibnitz FRM II, Technische Universität München, Lichtenbergstraße 1, D-85747 Garching b. München, Germany*

[6]*Institute for Material Science, Darmstadt University of Technology, D-64287 Darmstadt, Germany*

[7]*Institut für Anorganische Chemie, RWTH Aachen University, D-52074 Aachen, Germany*

(Received 20 January 2013; published 6 June 2013)

We present comprehensive investigations on a pyrochlore antiferromagnet $Na_3Co(CO_3)_2Cl$. Performed dc magnetization indicates a broad maximum at around 4 K. The field dependence of the peak temperature of this maximum follows the de Almeida–Thouless line, suggesting a spin-glass-like phase transition. The ac susceptibility measurements determine the glassy transition temperature to be 4.5 K and reveal a frequency-independent peak at 17 K. The temperature dependence of the specific heat shows a sharp peak at 1.5 K and a broad hump at around 5 K, which are attributed to a long-range magnetic phase transition and a spin-glass-like freezing process, respectively. The average crystallographic structure of $Na_3Co(CO_3)_2Cl$ has been determined using neutron-powder diffraction. No obvious site disorder has been detected within the experimental resolution. The diffuse neutron scattering with polarization analysis indicates short-range spin correlations characterized by dominating antiferromagnetic coupling between nearest neighbors and weak ferromagnetic coupling between next-nearest neighbors. The long-range magnetic order below 1.5 K is evidenced by the magnetic reflections observed at 50 mK and can be well explained with an all-in–all-out spin configuration. Inelastic neutron scattering of $Na_3Co(CO_3)_2Cl$ exhibits collective magnetic excitations at 3.5 K, suggesting that the spin-glass-like transition temperature $T_g = 4.5$ K does not correspond to a complete spin-glass freezing as expected in canonical spin glasses. The peak observed in magnetic susceptibility at 17 K is attributed to the onset of an intermediate partially ordered phase transition, qualitatively consistent with the theoretical predictions for pyrochlore antiferromagnets with weak ferromagnetic next-nearest-neighbor interactions.

DOI: 10.1103/PhysRevB.87.214406 PACS number(s): 75.50.Ee, 25.40.Dn, 78.70.Nx, 61.05.fg

I. INTRODUCTION

Magnetic structures which combine both antiferromagnetism and lattice symmetries based on triangles and tetrahedra inhibit the formation of a collinear ordered state and often display the phenomena known as geometrical frustration.[1–3] The best-known examples are two-dimensional kagome lattices and three-dimensional pyrochlore lattices. When antiferromagnetism is combined with magnetic pyrochlores, geometrical magnetic frustration is often expected from these tetrahedra-based structures and leads to unusual physical properties, attracting intensive research interest.[4] Anderson[5] and Villain[6] predicted high ground-state degeneracy and no long-range order at any temperature for Ising and Heisenberg spins with antiferromagnetic interactions on a pyrochlore lattice. But, it has been reported that some pyrochlore antiferromagnets exhibit long-range magnetic order as a result of the intriguing mechanism known as "order by disorder."[7–10] In some cases, additional degeneracy-lifting perturbations, e.g., further neighbor interactions, can also introduce long-range-ordered ground states in pyrochlore magnets.[11–13]

The best-studied family of pyrochlore magnets by now is the cubic pyrochlore oxides with the general chemical formula $A_2B_2O_7$,[14] which have dominated much of the literature due to a wide variety of interesting unusual ground states observed, such as spin glasses,[15–17] spin liquids,[18–20] and spin ices.[21,22] It is a somewhat surprising result that spin-glass-like behavior has been observed in a few examples of pyrochlore magnets, which are periodic, chemically ordered within the sensitivity of diffraction methods,[16,17,23–25] whereas, the received wisdom generally assumes that the formation of a spin-glass phase requires both chemical disorder and competing (or frustrated) interactions.[26,27] The origin of this spin-glass-like behavior has been the subject of an intense debate and has not yet been completely understood.[28,29] It was found that quantum fluctuations in the spin interactions play an important role in this glassy behavior.[30–33] On the other hand, although little evidence for site disorder among the cations or for significant vacancy concentrations on the oxygen sites was found in the spin-glass pyrochlore $Y_2Mo_2O_7$,[34,35] a subtle nonrandom distortion of the Mo sublattice was revealed by means of x-ray-absorption fine-structure (XAFS) measurement and nuclear magnetic resonance investigations.[36,37] Greedan *et al.* reported the neutron diffraction and neutron pair distribution function analysis on $Y_2Mo_2O_7$ and found that the principal source of

disorder is associated with the Y-O1 atom pairs rather than the Mo-Mo pairs, in disagreement with the result of XAFS measurement.[38] Ofer *et al.* detected a lattice deformation of $Y_2Mo_2O_7$ within the unit cell when approaching the spin-glass-like transition temperature using field-dependent nuclear and muon magnetic resonances, indicating that magnetoelastic coupling plays a role in the freezing process of $Y_2Mo_2O_7$.[39]

Herein, we report a new spin-frustrated compound that is formulated as $Na_3Co(CO_3)_2Cl$, whose structure features a three-dimensional anionic backbone of Co^{2+} carbonate, accommodating the sodium and chloride ions [see Fig. 1(a)]. Magnetic Co^{2+} ions are located at the corners of a network of corner-sharing tetrahedra, i.e., pyrochlore lattice, as shown in Fig. 1(b). The nearest-neighbor Co^{2+} ions are antiferromagnetically coupled, which leads to a high degree of magnetic frustration (see context below). In the present paper, $Na_3Co(CO_3)_2Cl$ is extensively investigated by means of dc magnetization and ac susceptibility, specific heat, neutron-powder diffraction (NPD), polarized neutron scattering, and inelastic neutron-scattering measurements. This research reveals the coexistence of a long-range magnetic order, an intermediate partially ordered magnetic phase, and a spin-glass-like transition, in one magnetic pyrochlore system $Na_3Co(CO_3)_2Cl$. The observed complex magnetic behaviors may extend the knowledge on the physics of pyrochlore magnets and geometrical spin frustration.

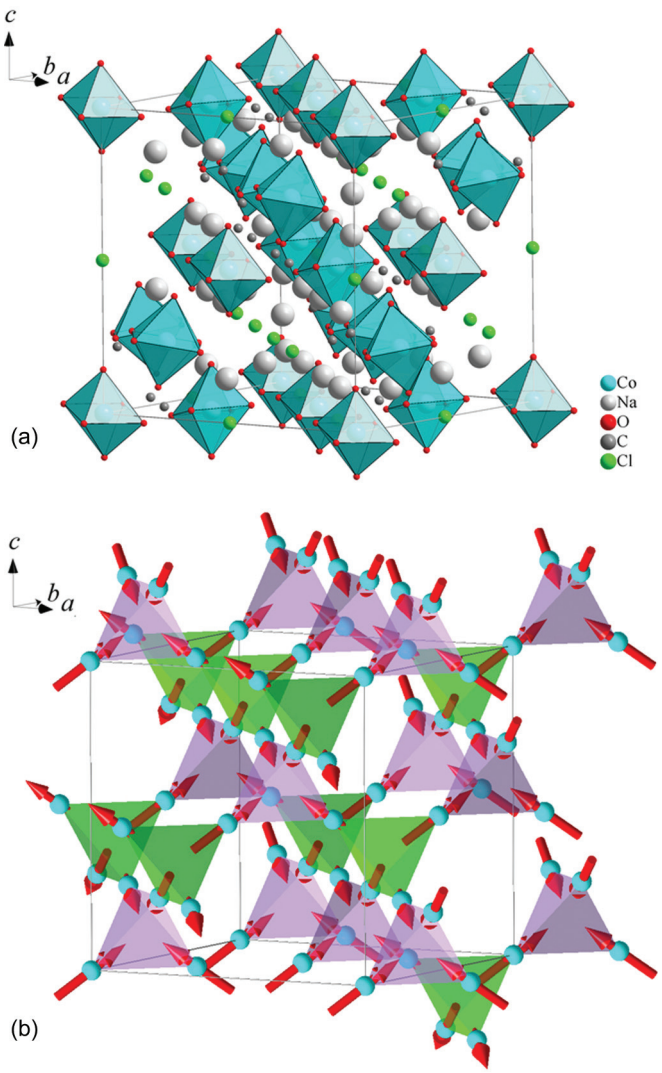

FIG. 1. (Color online) (a) Crystal structure of $Na_3Co(CO_3)_2Cl$ (cyan spheres: Co; light gray spheres: Na; red spheres: O; dark gray spheres: C; and green spheres: Cl). (b) Pyrochlore lattice of Co^{2+} ions (cyan spheres) with the all-in–all-out spin arrangements. The all-in and all-out spin tetrahedra are highlighted as purple and green, respectively.

II. EXPERIMENTAL DETAILS

The synthesis procedure of $Na_3Co(CO_3)_2Cl$ is summarized as follows. A mixture of $CoCl_2 \cdot 6H_2O$ (5.9 g, 0.025 mol), 1,10-phenanthroline (10.0 g, 0.05 mol), Na_2CO_3 (2.5 g, 0.025 mol), ethanol (72 ml), and water (6 ml) were stirred in the air for 10 min and then were transferred to a 110-ml Teflon-lined autoclave, which was heated to 160 °C for 96 h, followed by cooling to room temperature with a rate of 5 °C/h. The resulting pink polycrystalline products were washed by a large amount of ethanol/water, yielding 3.0 g (85%). Elemental analysis showed very little contamination by other transition-metal ions (less than 0.01%).

Neutron-powder-diffraction data for the refinement of the crystal structure were collected on the high-resolution diffractometer SPODI (Ref. 40) at the Forschungs-Neutronenquelle Heinz Maier-Leibnitz (FRM II) research reactor (Garching, Germany). For the measurements on SPODI, a Ge(551) monochromator was used to produce a monochromatic neutron beam with a wavelength of 1.5483 Å. The $Na_3Co(CO_3)_2Cl$ powder was filled in a thin wall vanadium container and then was mounted in a top-loading closed-cycle refrigerator. The FULLPROF package[41] was used for the Rietveld refinement of the crystal structure of $Na_3Co(CO_3)_2Cl$. The dc magnetization was measured using a superconducting quantum interference device magnetometer. The ac susceptibility and specific heat measurements were carried out using a physical property measurement system. Unable to synthesize a large crystal by now, $Na_3Co(CO_3)_2Cl$ powder was compressed with a load of 10-kbar pressure and a piece of compressed plate of 0.2-mm thickness, and a 1-mg mass was used for specific heat measurements. The polarized neutron-scattering measurements were carried out on the diffuse neutron spectrometer[42] (DNS) at FRM II, equipped with a ^{4}He closed-cycle cryostat and a dilution-insert cryostat, allowing a temperature range between 50 mK and 300 K. The energy of the incident neutron beam was 3.6 meV (corresponding to a wavelength of 4.74 Å). Within the quasistatic approximation, the nuclear coherent, spin-incoherent, and magnetic scattering cross sections are separated simultaneously with the *xyz*-polarization method in the spin-flip (SF) and non-spin-flip (NSF) channels.[43] In the *xyz*-polarization analysis, the multidetectors of the DNS define the *x*-*y* plane, which makes the scattering vector $\boldsymbol{Q}$ always perpendicular to the *z* direction. The SF and NSF differential cross sections are then measured for an *xyz*-polarized incident beam, giving a total of six partial cross sections, labeled $d\sigma_{\mathrm{SF}}^{(x,y,z)}/d\Omega$ and $d\sigma_{\mathrm{NSF}}^{(x,y,z)}/d\Omega$. The quantitative value of the differential magnetic cross section $d\sigma_{\mathrm{Mag}}/d\Omega$ in units of b sr^{-1} f.u.$^{-1}$ (where f.u. represents formula units) can be

extracted from either $\frac{d\sigma_{\rm mag}}{d\Omega} = 2(\frac{d\sigma^x_{\rm SF}}{d\Omega} + \frac{d\sigma^y_{\rm SF}}{d\Omega} - 2\frac{d\sigma^z_{\rm SF}}{d\Omega})$ or $\frac{d\sigma_{\rm mag}}{d\Omega} = 2(2\frac{d\sigma^z_{\rm NSF}}{d\Omega} - \frac{d\sigma^x_{\rm NSF}}{d\Omega} - \frac{d\sigma^y_{\rm NSF}}{d\Omega})$.[43] The two expressions correspond to independent measurements, and the magnetic differential cross section is taken as their average after verifying their equivalence to check for systematic errors. The powder sample for the DNS measurements was sealed under a helium atmosphere into an aluminum holder and a copper holder for use in the ^{4}He closed-cycle cryostat and the dilution-insert cryostat, respectively. The scattering from empty sample holders was subtracted from the raw data. The scattering intensities from the sample were normalized to the incoherent scattering of a vanadium standard to acquire the absolute scattering cross section. The flipping ratio was corrected by using the reference measurements from an ideal isotropic incoherent scatterer, a NiCr alloy. The inelastic neutron-scattering spectra were recorded using the multi-disc chopper high-resolution time-of-flight spectrometer TOFTOF (Ref. 44) at FRM II. TOFTOF covers scattering angles ranging from -15° to -7.5° and from 7.5° to 140°. The incident wavelength was 4.2 Å. The chopper rotation frequency was set to 14 000 rpm, resulting in an instrumental resolution of about 130 μeV full width at half maximum (FWHM) at zero energy transfer. The instrumental resolution function of TOFTOF was determined by the measurement at 250 K on a vanadium standard. About 5 g of $Na_3Co(CO_3)_2Cl$ powder was sealed in a hollow-cylinder aluminum sample holder under a helium atmosphere. The raw data were treated by subtracting the scattering from the empty sample holder and normalizing to the vanadium scan.

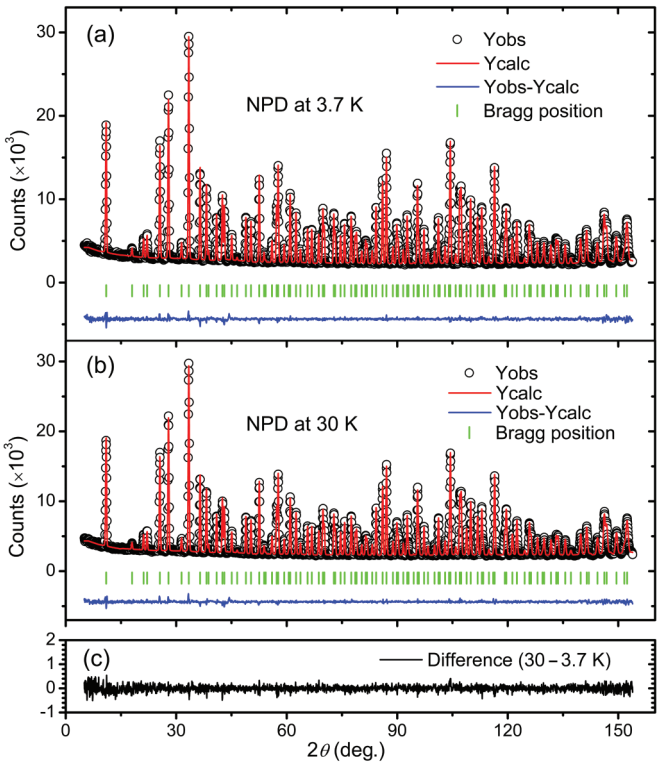

FIG. 2. (Color online) Experimental (Yobs), calculated (Ycalc), and difference (Yobs-Ycalc) NPD patterns obtained at (a) 3.7 K and (b) 30 K with the Rietveld refinement. The green short lines indicate the positions of the Bragg reflections. (c) Difference pattern between the data for 3.7 and 30 K.

III. EXPERIMENTAL RESULTS

A. Neutron-powder diffraction

X-ray single-crystal diffraction shows that $Na_3Co(CO_3)_2Cl$ crystallizes in cubic structure with space group $Fd\bar{3}$ (No. 203) and lattice constant $a = 13.9959(5)$ Å at 123 K.[45] In order to confirm the crystal structure more precisely and to detect possible defect structures, we performed NPD measurements at various temperatures from 3.7 to 300 K. The experimental NPD patterns (black circles) for 3.7 and 30 K are shown in Figs. 2(a) and 2(b), respectively, together with the Bragg positions (green short lines), the calculated patterns (red lines,) and the differences (blue lines) between the experimental and the calculated patterns. The calculated patterns are in good agreement with the experimental ones. The difference profile obtained by subtracting the experimental pattern for 3.7 K from the one for 30 K is plotted in Fig. 2(c), showing no sign for any long-range magnetic phase transition existing between these two temperatures.

In the Rietveld refinement of crystal structure, the best agreement between the NPD data and the structural model has been found when Co has been modeled occupying the 16*c* (0,0,0) site, C occupying the 32*e* $(x + 0.25, -x, x + 0.25)$ site, Cl occupying the 16*d* (0.25,0.25,0.5) site, O occupying the 96*g* (x, y, z) site, and Na occupying the 48*f* (0.125,*y*,0.125) site. Considering the experimental accuracy, the occupancies of all atoms are set as 1 because the change in occupation numbers is less than 10% if they are refined.[46] Although the Co sublattice displays a fully ordered pyrochlore, displacement on Na sites is obvious in the sense that the *y* position slightly deviates from -0.125 as expected for the ordered phase. The Co and C atoms are refined with the isotropic model. The use of anisotropic atomic displacement parameters on the Na, O, and Cl sites results in a significant improvement of the residuals of the refinement, especially at higher temperatures. Due to symmetry constraints, the anisotropic atomic displacement parameters for the Na, O, and Cl sites were modeled as Na (u_{11},u_{22},u_{33},$u_{12} = u_{23} = 0$,u_{13}), O (u_{11},u_{22},u_{33},u_{12},u_{23},u_{13}), and Cl ($u_{11} = u_{22} = u_{33}$, $u_{12} = -u_{23}$, and $u_{12} = -u_{13}$). The best fits to the NPD patterns for 3.7, 30, and 300 K are obtained with the structure parameters, reliability factors, and atomic displacement parameters summarized in Table I.

The atomic displacement parameters can indicate static disorder, an essential ingredient for the spin-glass behavior in addition to magnetic frustration. At the lowest temperature, the sequence of mean-atomic displacement factors of $Na_3Co(CO_3)_2Cl$ follows $u_{\rm eq}({\rm Na}) \geqslant u_{\rm eq}({\rm Cl}) \geqslant u_{\rm eq}({\rm C}) \geqslant u_{\rm eq}({\rm Co})$, whereas, the weight of the constituents in $Na_3Co(CO_3)_2Cl$ (usually inversely proportional to the mean amplitude of thermal vibrations) reads as $m_{\rm Na} < m_{\rm C} < m_{\rm Cl} < m_{\rm Co}$, which might indicate some static atomic disorder on the chlorine site.

In Fig. 3, the temperature dependence of the unit-cell volume is plotted, and it is modeled following the Grüneisen approximation for the zero pressure state where the effects of thermal expansion are considered to be equivalent to elastic strain.[47] The temperature dependence of the unit-cell volume

TABLE I. Lattice parameters, reliability factors, and anisotropic atomic displacement parameters of $Na_3Co(CO_3)_2Cl$ at 3.7, 30, and 300 K. The errors are statistical errors given by the FULPROF program. The bound coherent scattering length for the elements in $Na_3Co(CO_3)_2Cl$ are as follows: $b_{Na} = 3.63$, $b_{Co} = 2.49$, $b_C = 6.646$, $b_O = 5.803$, and $b_{Cl} = 9.577$ fm (Ref. 46).

		3.7 K	30 K	300 K
$a = b = c$ (Å)		13.9898(1)	13.9898(3)	14.0433(1)
$\alpha = \beta = \gamma$ (Å)		90	90	90
V (Å^3)		2738.011(21)	2738.011(22)	2769.511(29)
Na	y/b	−0.1510(5)	−0.1510(3)	−0.1502(2)
O	x/a	−0.0243(6)	−0.0243(7)	−0.0230(9)
	y/b	0.6469(8)	0.6469(3)	0.6469(9)
	z/c	0.5165(3)	0.5165(8)	0.5158(1)
C	x/a	0.0326(5)	0.0326(5)	0.0327(7)
Reliability factors (%)				
R_{wp}		6.75	6.87	7.09
R_p		7.06	7.29	8.32
R_B		1.77	1.81	1.90
χ^2		0.871	0.893	0.665
Anisotropic displacement parameters ($\times 10^{-3}$ Å^2)				
Co	u_{iso}	0.138(25)	0.097(24)	0.648(36)
C	u_{iso}	0.245(8)	0.227(8)	0.657(10)
Na	u_{11}	0.55(8)	0.60(8)	1.64(11)
	u_{22}	0.48(7)	0.48(7)	1.64(11)
	u_{33}	0.67(7)	0.79(7)	2.03(10)
	u_{13}	0.14(6)	0.17(6)	−0.22(9)
Cl	u_{11}	0.58(2)	0.60(2)	2.61(4)
	u_{12}	0.18(3)	0.16(3)	1.11(5)
O	u_{11}	0.39(4)	0.33(4)	1.19(6)
	u_{22}	0.33(3)	0.36(3)	0.92(4)
	u_{33}	0.49(4)	0.51(4)	1.73(6)
	u_{12}	−0.20(2)	−0.18(2)	−0.45(3)
	u_{13}	0.08(2)	0.08(2)	0.11(3)
	u_{23}	−0.06(2)	−0.07(2)	−0.23(3)

can be expressed as $V(T) = \gamma U(T)/K_0 + V_0$, where γ is the Grüneisen parameter, K_0 is the bulk modulus, and V_0 is the hypothetical cell volume at 0 K. The internal energy $U(T)$ is given under the Debye approximation by

$$U(T) = 9Nk_BT\left(\frac{T}{\Theta_D}\right)^3 \int_0^{\Theta_D/T} \frac{x^3}{e^x - 1}dx, \qquad (1)$$

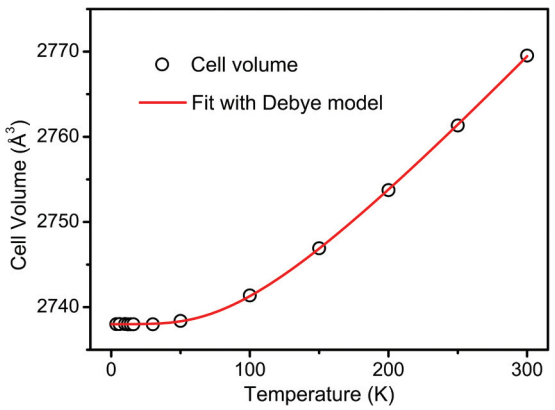

FIG. 3. (Color online) Temperature dependence of the unit-cell volume of $Na_3Co(CO_3)_2Cl$. The red line is the best fit with the Debye model as described in the text.

where N is the number of atoms per unit cell, k_B is the Boltzmann constant, and Θ_D is the Debye temperature. The best fit to the data yields $\gamma/K_0 = (1.88 \pm 0.03) \times 10^{-9}$ Pa^{-1}, $\Theta_D = 394.6 \pm 3.5$ K, and $V_0 = 2737.99 \pm 0.02$ Å^3. No discontinuity can be seen in the temperature dependence of the cell volume, suggesting no crystallographic phase transition over the investigated temperature range.

Thus, the average crystallographic structure of $Na_3Co(CO_3)_2Cl$ has been determined. No evidence for long-range magnetic order can be seen from 300 to 3.7 K. Note that, in Fig. 2, the background increases at low angles, just where magnetic scattering could be visible due to the form-factor behavior. But the magnetic scattering is too weak to be separated from the background. In Sec. III E, the magnetic scattering of $Na_3Co(CO_3)_2Cl$ will be measured using polarized neutron scattering and will be discussed in detail. Excellent refinements to the NPD data have been obtained without introducing any magnetic contribution. Static atomic disorder could possibly exist on the chlorine sites. However, no clear evidence for atomic disorders in $Na_3Co(CO_3)_2Cl$ has been observed within the resolution of our NPD measurements.

B. dc magnetization

Zero-field-cooled (ZFC) and field-cooled (FC) dc magnetization curves of $Na_3Co(CO_3)_2Cl$ were measured from 2 to

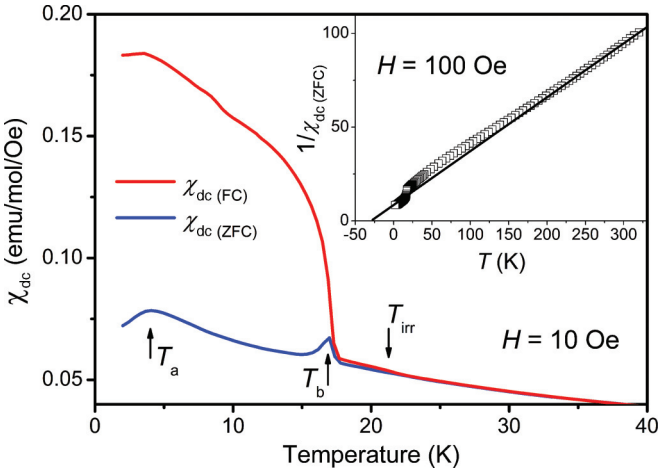

FIG. 4. (Color online) ZFC (blue line) and FC (red line) dc susceptibilities of $Na_3Co(CO_3)_2Cl$ at the temperature ranging from 2 to 40 K under a probing field of 10 Oe. T_a: temperature of the maximum of the hump in the ZFC susceptibility at around 4 K; T_b: inflection temperature suggesting the onset of the partial order; and T_{irr}: irreversibility temperature of the ZFC and FC susceptibility curves. Inset: temperature dependence of the inverse ZFC susceptibility with the best fit of the Curie-Weiss law.

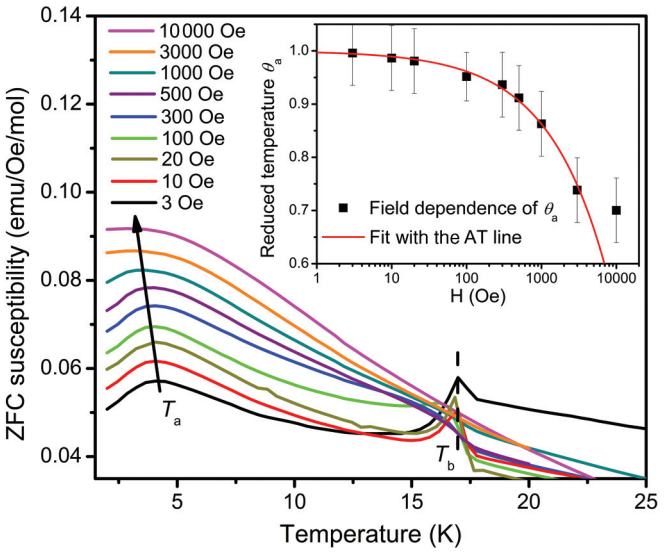

FIG. 5. (Color online) In the dc technique, ZFC susceptibility curves measured under various probing fields of 3, 10, 20, 100, 300, 500, 1000, 3000, and 10 000 Oe. The y axis corresponds to the data for 3 Oe. The data for other external fields are shifted for the sake of clarity. Inset: field dependence of the reduced temperature θ_a with the best fit in terms of the AT line (red line). T_a,T_b: see the caption for Fig. 4.

320 K under various probing fields. In a typical ZFC measurement, the sample was cooled down without an external field, and then, the magnetization M was measured with a probing field H. The FC magnetization data were collected while the sample was cooled down under an external field. In this paper, we define M/H as the dc susceptibility χ_{dc}. The temperature dependence of the ZFC susceptibility $\chi_{dc(ZFC)}$ and the FC susceptibility $\chi_{dc(FC)}$ under a probing field of 10 Oe is plotted in Fig. 4.

The ZFC and FC susceptibility curves diverge below an irreversibility temperature $T_{irr} \approx 21.4$ K. There is a hump in the ZFC susceptibility at around 4 K, whose peak temperature is defined as T_a. An inflection temperature appears at $T_b \approx 17$ K. The temperature dependence of the inverse ZFC susceptibility $1/\chi_{dc(ZFC)}$ was measured from 2 to 300 K under 100 Oe and is plotted in the inset of Fig. 4. The data above 220 K can be well fitted by the Curie-Weiss (CW) law, yielding a Curie-Weiss temperature $\Theta_{CW} = -33.8 \pm 5.2$ K and a Curie constant $C = 3.5 \pm 0.6$ emu K^{-1} Oe^{-1} mol^{-1}. The negative value of Θ_{CW} shows dominant antiferromagnetic coupling between Co^{2+} ions. In a mean-field approximation with nearest-neighbor interactions only, the Curie constant and the Curie-Weiss temperature, respectively, are given by[48]

$$C = \frac{9}{8}\left[\frac{N\mu_{eff}^2}{3k_B}\right] \quad \text{and} \quad \Theta_{CW} = \frac{3}{2}\left[\frac{zJS(S+1)}{3k_B}\right]. \qquad (2)$$

Here, μ_{eff} is the effective moment of a Co^{2+} ion, J is the exchange constant among the nearest neighbors, and $z = 6$ is the number of nearest neighbors. It is then estimated that $\mu_{eff} = 5.3 \pm 0.4\mu_B$ and $J = 0.26 \pm 0.05$ meV. The effective moment per Co^{2+} extracted from the dc susceptibility exceeds the spin-only value of $3.87\mu_B$ for Co^{2+} in the high spin state ($s = 3/2$), consistent with what has been reported in the literature.[49,50] The excess magnetic moment of Co^{2+} above the predicted spin-only value is due to the spin-orbital coupling contribution as often reported for Co^{2+} ions in octahedral crystal-field environments.[49,50]

The ZFC magnetization curves were measured under various probing fields as shown in Fig. 5. The scales of the x,y axes correspond to the data for 3 Oe. The curves for other fields are shifted along the y axis for the sake of clarity. In Fig. 5, the kink at $T_b = 17$ K decreases and finally disappears with increasing probing fields. There is a field-independent dip at T_b in the differential susceptibility (not shown here) for all probing fields. This inflection temperature T_b may reflect the onset of some kind of long-range collective behavior of the Co^{2+} spins. The hump at T_a (~4 K) gradually shifts to a lower temperature with increasing magnetic fields. The field dependence of T_a is investigated in terms of the de Almeida–Thouless (AT) line.[51] The AT line can be observed near the freezing temperature and associates with the onset of irreversibility of spin glasses on macroscopic time scales.[27]

The AT line can be obtained by plotting the reduced temperature $\theta_a = T_a/T_c$ versus the probing magnetic field H. T_c is the Curie temperature of the material, whereas, for a spin-glass system, T_c should be replaced by the zero-field spin-glass transition temperature T_g. The reduced temperature θ_a scales with H as the following expression:[51]

$$\theta_a \propto 1 - \frac{C_{AT}}{T_g}H^n. \qquad (3)$$

Here, C_{AT} is a constant, and $T_g = 4.5$ K (given later in the ac susceptibility results). The field dependence of the reduced temperature θ_a is plotted in the inset of Fig. 5. The best fit with Eq. (3) yields $n = 0.59 \pm 0.05$. In canonical spin-glass systems, the mean-field theory predicts $n = 2/3$,[51,52] which is close to the n value given in our results. At a large field of 10 000 Oe, a deviation from the AT line is observed in agreement with what has been reported that deviations

from the AT line may happen in some spin glasses under large magnetic fields.[53,54] Thus, the hump at T_a should stem from a spin-glass-like freezing process. The downshift in T_a with increasing magnetic fields makes sense because higher magnetic fields suppress the energy barriers and, thus, reduce the freezing temperature.

C. ac susceptibility

Spin-glass behavior is usually studied by the ac susceptibility, and the spin-glass transition temperature can be accurately determined by the frequency dependence of real or imaginary components.[26,55] The ac susceptibility measurement of $Na_3Co(CO_3)_2Cl$ was performed with an ac amplitude of $\mu_0 h_{ac} = 10$ Oe at the frequencies of $25 \leqslant f \leqslant 10^4$ Hz after ZFC from room temperature. The temperature dependence of the real component of the ac susceptibility χ' at different frequencies is plotted in Fig. 6. The inflection point in dc susceptibility at $T_b \approx 17$ K appears to be a peak in the ac susceptibilities for all frequencies, and its peak position is frequency independent, indicating this peak is not due to a spin-glass transition. Considering the sharp appearance of the low-field dc and ac susceptibilities at T_b, the system may undergo a long-range collective magnetic behavior at this temperature, although no long-range magnetic order is suggested by NPD measurements. The broad peak at around 4 K displays clear frequency dispersion. The temperature T_m at the maximum of this broad peak shifts to higher values as the frequency increases. The spin-glass-like transition is then evidenced by fitting the frequency dependence of the peak temperature to a critical power law,[26,55,56]

$$\tau = \tau^* \left(\frac{T_m}{T_g} - 1 \right)^{-zv}, \tag{4}$$

where $\tau = (2\pi f)^{-1}$, τ^* is the relaxation time of an individual particle moment, T_g is the static glassy transition temperature, and zv is the dynamic critical exponent. The best fit in terms of

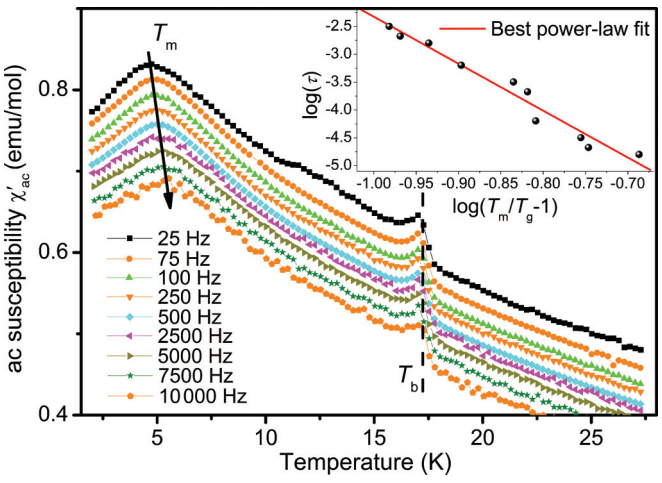

FIG. 6. (Color online) Temperature dependence of the real ac susceptibility component χ' at frequencies of $25 \leqslant f \leqslant 10\,000$ Hz. The y axis corresponds to the data for 25 Hz. The data for other frequencies are shifted for the sake of clarity. Inset: frequency dependence of the freezing temperature T_m with the best power-law fit (red line).

Eq. (4) is shown in the inset of Fig. 6, yielding $T_g = 4.5(4)$ K, $\tau^* = 10^{-10.7(5)}$ s, and $zv = 8.4(6)$. For the sake of clarity, the inset of Fig. 6 is plotted in the style of $\log(\tau)$ versus $\log(T_m/T_g - 1)$. The value of zv holds well in the range between 4 and 12 found in the spin-glass materials.[26,56] The value of relaxation time $\tau^* = 10^{-10.7(5)}$ s also locates in the characteristic range of 10^{-8}–10^{-12} s, usually derived for canonical spin glass.[26,56,57]

Another important factor used for quantitatively characterizing a magnetic glassy transition is the frequency shift K, which gives a relative variation in the peak temperature T_m with the angular frequency ω and often offers a good criterion for distinguishing a canonical spin glass from a superparamagnet. The frequency shift K is defined as $(\Delta T_m/T_m)$ per decade ω as follows:[26,55]

$$K = \frac{1}{T_m} \frac{\Delta T_m}{\Delta \, log \, \omega}. \tag{5}$$

Using Eq. (5), the frequency shift K on $Na_3Co(CO_3)_2Cl$ is estimated to be about 0.04, much smaller than the values for superparamagnets and close to those observed in spin glasses.[26]

D. Specific heat

The temperature dependence of the specific heat of $Na_3Co(CO_3)_2Cl$ was measured under a zero external field within the temperature range of 90 mK to 220 K as shown in Fig. 7(a). Without a nonmagnetic reference material, it is difficult to determine the lattice specific heat precisely. However, a simple Debye model may describe the lattice specific heat $C_{lattice}$ nicely as shown by the red line in Fig. 7(a), which is expressed in the conventional form[58]

$$C_{Debye} = 9sR \left(\frac{T}{\Theta_D} \right)^3 \int_0^{\Theta_D/T} \frac{x^4 e^x dx}{(e^x - 1)^2}, \tag{6}$$

where s is the number of atoms per formula unit, R is the ideal gas constant, and Θ_D is the Debye temperature. The best fit with the Debye model yields a Debye temperature of $\Theta_D = 380 \pm 20$ K, close to the value obtained in the NPD measurements. The inset of Fig. 7(a) shows the specific heat data on a log-log scale where a clear upturn can be seen below 0.25 K. This upturn is attributed to the high-temperature tail of the theoretical hyperfine contribution due to the nonzero magnetic moments of the ^{59}Co nucleus. The hyperfine interaction gives rise to a Schottky specific heat anomaly with the high-temperature tail given by[59]

$$C_{hf} = R \frac{I(I+1)}{3} \left(\frac{g_n \mu_N H_{hf}}{k_B T} \right)^2, \tag{7}$$

where $I = 7/2$ is the nuclear spin of ^{59}Co with 100% natural abundance, g_n is the nuclear g factor, μ_N is the nuclear magneton, and H_{hf} is the effective hyperfine field. The fit using Eq. (7) was performed with the specific heat data below 0.25 K where the hyperfine contribution becomes overwhelming as compared to the lattice and electronic-spin contributions. The best fit is shown as the blue line in the inset of Fig. 7(a) and yields an effective hyperfine field in $Na_3Co(CO_3)_2Cl$, $H_{hf} = 250(10)$ kOe. The magnetic specific heat is then obtained by subtracting both the lattice contribution $C_{lattice}$ and the hyperfine contribution C_{hf} from the total specific heat. Figure 7(b) shows the magnetic specific heat below 19 K. The

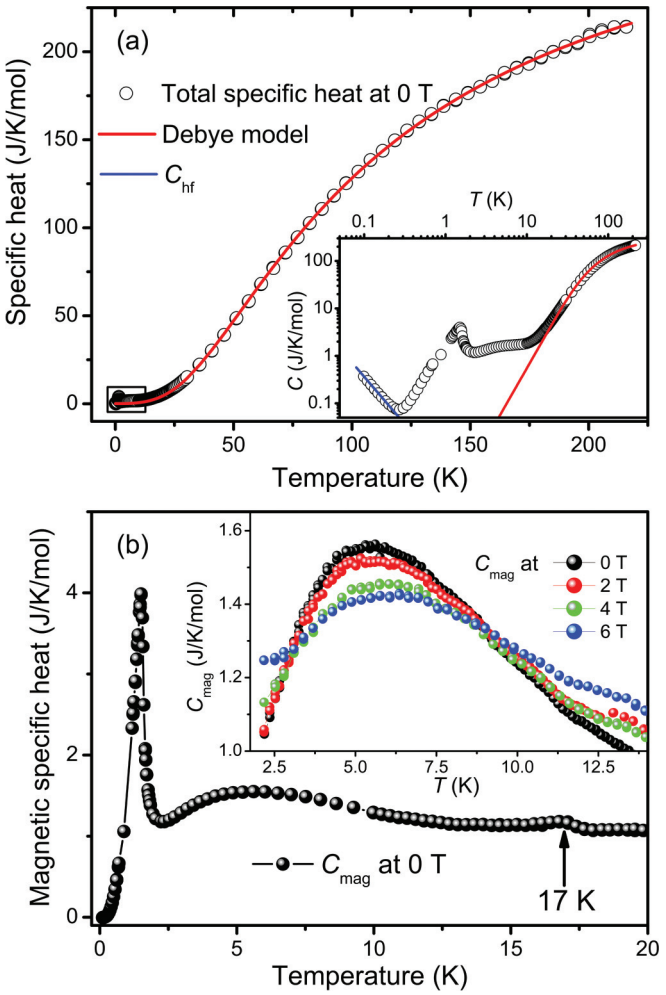

FIG. 7. (Color online) (a) Temperature dependence of the specific heat of $Na_3Co(CO_3)_2Cl$ under a zero external magnetic field with the fit of a simple Debye model (red line) and a hyperfine interaction (blue line) on a linear-linear scale and (inset) a log-log scale. (b) Magnetic specific heat under 0 T. Inset of (b): Magnetic specific heat under 0, 2, 4, and 6 T within the temperature range from 2 to 14 K.

most striking features in this region are a small hump at ∼17 K, a broad hump at ∼5 K, and a sharp λ-shaped peak at 1.5 K. The small hump at ∼17 K should correspond to the inflection temperature T_b found in the magnetic susceptibility measurements, suggesting a long-range collective spin behavior. The hump at ∼5 K should be due to the spin-glass-like transition at T_g = 4.5(4) K since spin-glass systems normally exhibit a broad maximum in magnetic specific heat with the peak temperature $T_{max} \approx 1.3T_g$. For canonical spin glasses, this broad maximum above T_g decreases slowly with increasing temperature and shifts towards higher temperatures with an increasing external field.[26] The magnetic specific heat of $Na_3Co(CO_3)_2Cl$ was measured under various external fields and was plotted in the inset of Fig. 7(b). The hump at ∼5 K shifts to higher temperatures and smears out as the external magnetic field increases, which is consistent with the behavior of canonical spin glasses.

The sharp peak at 1.5 K in Fig. 7(b) is attributed to a long-range magnetic phase transition. Unfortunately, it is not applicable to carry out a precise fit to the sharp peak at 1.5 K and the broad hump at ∼5 K. First, they are too close to be

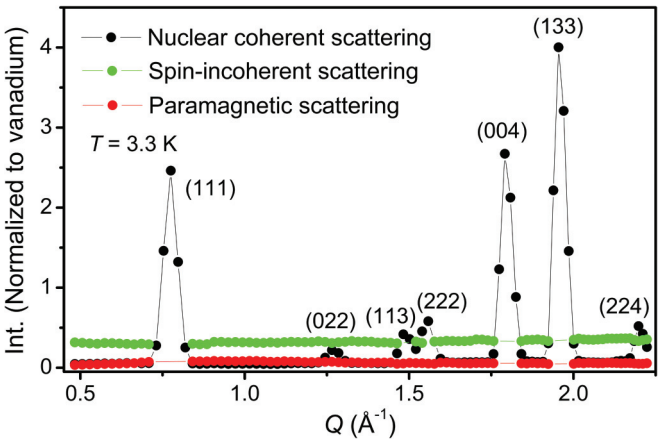

FIG. 8. (Color online) Nuclear coherent (black circles), spin-incoherent (green circles), and magnetic (red circles) contributions to the total diffuse neutron scattering from $Na_3Co(CO_3)_2Cl$ at 3.3 K separated by *xyz*-polarization analysis on the DNS.

fitted separately. Second, the hump at ∼5 K associates with the spin-glass-like freezing of Co^{2+} spins so that a Schottky-type magnetic specific heat model is inappropriate since a probability distribution of energy splitting, rather than several well-defined energy gaps, has to be considered for spin-glass systems.[25,60] Accordingly, the frustration parameter $f = |\Theta_{CW}|/T_N \approx 22.5$ (Ref. 2) can be determined and attributes $Na_3Co(CO_3)_2Cl$ to the family of highly frustrated magnets.

E. Diffuse neutron scattering with a polarization analysis

As discussed above, we have observed clear collective magnetic behavior in $Na_3Co(CO_3)_2Cl$. At low temperatures, the spins should become antiferromagnetically correlated. Therefore, spin correlations are normally expected from such spin systems, appearing as a modulation in the differential scattering cross section in a neutron-scattering experiment. In order to detect the short-range spin correlations and the long-range magnetic order in $Na_3Co(CO_3)_2Cl$, diffuse neutron scattering with a polarization analysis was performed at the DNS, FRM II.

Figure 8 shows the nuclear coherent (black circles), spin-incoherent (green circles), and magnetic (red circles) components of the total scattering from $Na_3Co(CO_3)_2Cl$ at 3.3 K by means of *xyz*-polarization analysis on the DNS. The data were collected within the Q range from 0.4 to 2.2 Å^{-1}. The spin-incoherent scattering intensity is nearly constant, suggesting a successful separation of the different scattering contributions. Obviously, the magnetic contribution is weak as compared with the nuclear and spin-incoherent scatterings and could hardly be seen without polarization analysis. The gaps in the spin-incoherent and magnetic data are due to the imperfect separations caused by the strong Bragg peaks at those positions.

Figure 9 shows the differential magnetic cross section $d\sigma_{mag}/d\Omega$ extracted from the total scattering cross section at 0.05, 3.3, 10, 30, 200, and 300 K. There is no trace of long-range magnetic order down to 3.3 K, consistent with the NPD measurements. At 50 mK, long-range magnetic order is evidenced by clear magnetic Bragg peaks superposed on the magnetic diffuse scattering, confirming that the sharp peak

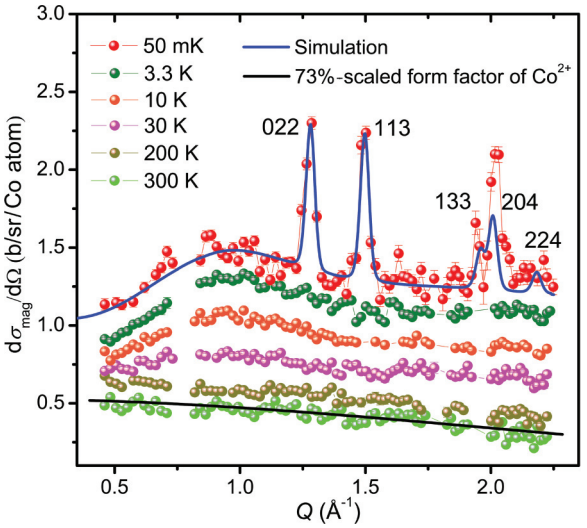

FIG. 9. (Color online) Temperature evaluation of the differential magnetic cross section. The x and y axes correspond to the data for 200 and 300 K. The data at other temperatures are displaced vertically by 0.2 b sr^{-1} per Co atom for clarity. The black line indicates the 73%-scaled paramagnetic form factor of the Co^{2+} ion ($S = 3/2$). The blue line is the best fit to the magnetic scattering at 50 mK based on the all-in–all-out spin configuration.

at 1.5 K in specific heat can be attributed to a magnetic phase transition into a long-range-ordered antiferromagnetic structure. The scattering cross section at 300 K agrees well with the 73%-scaled paramagnetic form factor of the Co^{2+} ($S = 3/2$) ion. Without an energy analysis option, the magnetic scattering data taken on the DNS are actually integrated within the energy-transfer window of the DNS. The overall energy scale of the magnetic exchange in this system extends to about 3 meV (see the next section), which is basically covered by the energy window (3.6 meV) of the DNS. About 27% of the magnetic scattering intensity cannot be retrieved because of the limitation of the energy window of the DNS.

The effect of the magnetic short-range order can be seen as a modulation in the differential scattering cross section in Fig. 9. The strong reduction in the magnetic cross section below $Q \approx 0.9$ Å^{-1} indicates the existence of a strong antiferromagnetic component in the spin correlations in agreement with the aforementioned susceptibility measurements of $Na_3Co(CO_3)_2Cl$.

The data collected at 3.3 K (below the spin-glass-like transition temperature and above the long-range magnetic ordering temperature) were used for the analysis of the short-range spin correlations as shown by the red circles in Fig. 10. The differential magnetic scattering cross section of $Na_3Co(CO_3)_2Cl$ can be calculated with the formula given by Blech and Averbach for the differential scattering cross section of spin pairs, which, already in powder average, can be written as[61]

$$\frac{d\sigma_{\mathrm{mag}}}{d\Omega} = \frac{2}{3}S(S+1)\left(\frac{\gamma e^2}{mc^2}\right)^2 f^2(Q) + \left(\frac{\gamma e^2}{mc^2}\right)^2 f^2(Q)\sum_{n=1}^{N} c_n\left[a_n\frac{\sin Qr_n}{Qr_n} + b_n\left(\frac{\sin Qr_n}{Q^3r_n^3} - \frac{\cos Qr_n}{Q^2r_n^2}\right)\right], \quad (8)$$

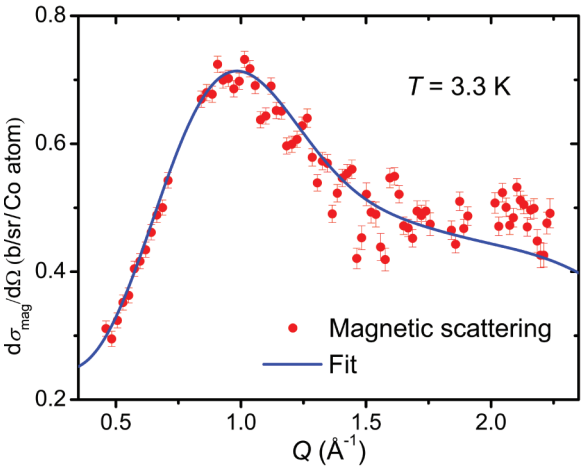

FIG. 10. (Color online) Differential magnetic scattering cross section at 3.3 K in absolute units (red circles) with the best fit (blue line) in terms of Eq. (10).

where $\frac{\gamma e^2}{mc^2} = -0.54 \times 10^{-12}$cm is the magnetic scattering length, S is the spin quantum number of the scattering ion, $f(Q)$ is the magnetic scattering form factor, and it is assumed that an arbitrary reference Co^{2+} ion is correlated to N surrounding Co^{2+} shells with occupation number c_n and shell radius r_n. a_n and b_n are related to the probability of finding spin pairs with parallel components and are expressed as follows:[61]

$$a_n = \langle \boldsymbol{S}_0^{\boldsymbol{y}} \cdot \boldsymbol{S}_n^{\boldsymbol{y}} \rangle_n, \qquad b_n = 2\langle \boldsymbol{S}_0^{\boldsymbol{x}} \cdot \boldsymbol{S}_n^{\boldsymbol{x}} \rangle_n - \langle \boldsymbol{S}_0^{\boldsymbol{y}} \cdot \boldsymbol{S}_n^{\boldsymbol{y}} \rangle_n . \quad (9)$$

Here, $\langle \boldsymbol{S}_0^{\boldsymbol{\alpha}} \cdot \boldsymbol{S}_n^{\boldsymbol{\alpha}} \rangle_n$ is the average correlation of the $\boldsymbol{\alpha}$-direction component of the nth shell to the corresponding component of the origin spin. Denote $A_n = \langle \boldsymbol{S}_0^{\boldsymbol{x}} \cdot \boldsymbol{S}_n^{\boldsymbol{x}} \rangle_n$ and $B_n = \langle \boldsymbol{S}_0^{\boldsymbol{y}} \cdot \boldsymbol{S}_n^{\boldsymbol{y}} \rangle_n$. Then, Eq. (8) becomes

$$\frac{d\sigma_{\mathrm{mag}}}{d\Omega} = \left(\frac{\gamma e^2}{mc^2}\right)^2 f^2(Q)\left\{\frac{2}{3}S(S+1) + \sum_{n=1}^{N} c_n\left[B_n\frac{\sin Qr_n}{Qr_n} + (2A_n - B_n) \times \left(\frac{\sin Qr_n}{Q^3r_n^3} - \frac{\cos Qr_n}{Q^2r_n^2}\right)\right]\right\}. \quad (10)$$

Due to the glassy nature of this spin system at 3.3 K, an analytical simulation of the spin correlations has been carried out by attempting a least-squares fit with Eq. (10) to the magnetic differential scattering cross section obtained at 3.3 K. The best fit was achieved with two Co^{2+} shells, namely, $c_n =$ 6,12 for $n =$ 1,2, shown as the blue line in Fig. 10. If the higher-order shells ($n > 2$) were included, the corresponding A_n and B_n were so small that the correlations between the origin and the $n > 2$ shells can be neglected. This agrees with the estimation of the correlation length using the peak at $Q \approx 1.0$ Å^{-1}, whose FWHM is $\Delta Q \approx 1.0$ Å^{-1} and approximately corresponds to the next-nearest-neighbor distance. The best fit yields $A_1 = -0.14(3)$, $B_1 = -0.05(1)$, $A_2 = 0.04(2)$, and $B_2 = 0.01(1)$. The values of A_1 and B_1 are negative, indicating the nearest-neighbor Co^{2+} ions are antiferromagnetically coupled. Weak ferromagnetic coupling (A_2,$B_2 > 0$) is found among the

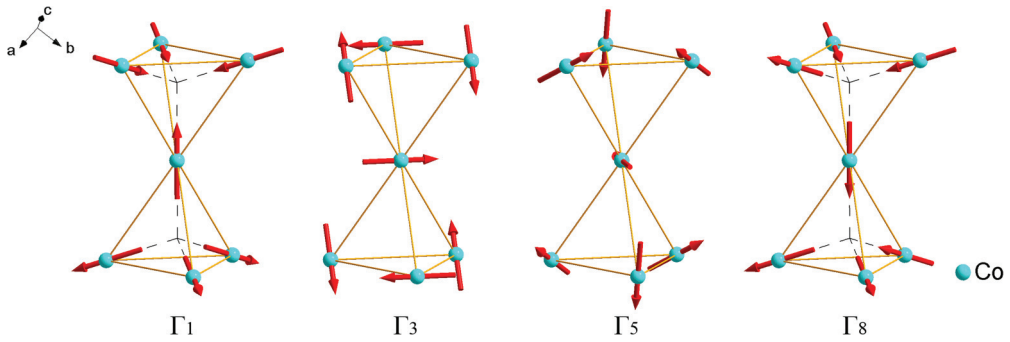

FIG. 11. (Color online) Schematic of a fragment of four possible ordered arrangements of Co spins in the low-temperature pyrochlore phase. Γ_1: all-in–all-out spin configuration. Γ_3: noncollinear spin configuration with Co spins confined in the *ab* plane and pointed to the [± 1 ± 1 0] directions. Γ_5: noncollinear spin configuration with Co spins pointed parallel to the [± 1/2 ± 1/2 ± 1] directions. Γ_8: spin ice structure with a two-in–two-out spin configuration.

next-nearest neighbors. A_2 and B_2 are quite small compared with A_1 and B_1, indicative of dominating nearest-neighbor antiferromagnetic correlations.

As for the long-range magnetic order of $Na_3Co(CO_3)_2Cl$ at 50 mK, two clear magnetic Bragg peaks have been observed at 1.27 and 1.50 $Å^{-1}$ as superpositions of the (220) and (113) nuclear Bragg peaks, respectively. This suggests an antiferromagnetic-ordered structure with propagation vector $q_0 = (0,0,0)$. Two further magnetic peaks are observed at 1.93 and 2.03 $Å^{-1}$, which could correspond to the magnetic (133) and (204) reflections. But we are not confident about these two reflections due to the strong affection of the (133) nuclear reflection. Symmetry analysis, based on representation theory, indicates that the magnetic representation for magnetic Co^{2+} on the 16*c* site is decomposed into three one-dimensional irreducible models Γ_1, Γ_3, and Γ_5, and one three-dimensional irreducible model Γ_8. Four possible magnetic structures corresponding to four different magnetic representations are displayed in Fig. 11. The representations Γ_3, Γ_5, and Γ_8 can be ruled out directly because all these three models yield considerable intensity for the magnetic (111) reflection, whereas, the (111) reflection does not exist as indicated in our DNS data taking into account the relative intensity of the nuclear and the magnetic reflections. The representation Γ_1 with the all-in–all-out spin configuration leads to zero intensity for the (111) magnetic reflection. Therefore, the fitting to the magnetic reflections has been carried out based on the all-in–all-out spin configuration [see Fig. 1(b)] where the spins in one tetrahedron direct either towards or opposite the center of the tetrahedron. The fitting result is plotted in Fig. 9 as the blue line. The two prominent reflections (220) and (113) are well fitted. An additional magnetic reflection (224) presents at $Q = 2.18$ $Å^{-1}$ in the simulation, which is hard to identify in the DNS data due to its weak intensity. Given the fact that the calculated diffraction pattern, based on the all-in–all-out magnetic structural model, fits well with our experimental data, we can safely conclude that the long-range magnetic order of $Na_3Co(CO_3)_2Cl$ is characterized by an all-in–all-out-type spin configuration. Note that the emergence of a similar noncollinear antiferromagnetic ground state has been reported in some pyrochlore magnets.[62–65] As shown in Fig. 9, there is still significant magnetic diffuse scattering at 50 mK in addition to the magnetic reflections. One explanation could be that $Na_3Co(CO_3)_2Cl$ enters a partially ordered ground state within the experimental time window owing to its slow magnetic relaxation. But temperature inhomogeneity could also lead to the magnetic diffuse scattering observed at 50 mK because the DNS measurements were performed on a large quantity of powder samples. A precise determination of the magnetic ground state of $Na_3Co(CO_3)_2Cl$ will be interesting and, in the future, will require more neutron-scattering studies on single crystals below 1.5 K.

Thus, polarized neutron-scattering investigations show that significant spin correlations build up below 30 K. The analysis of spin correlations indicates that the spin structure of this system is characterized by dominating antiferromagnetic coupling among the nearest neighbors with weak ferromagnetic next-nearest-neighbor interaction. Magnetic Bragg peaks, observed at 50 mK, indicate that $Na_3Co(CO_3)_2Cl$ enters an all-in–all-out long-range magnetic order (or partial order) below 1.5 K.

F. Inelastic neutron scattering

Inelastic neutron scattering (INS) provides a rather unique probe of collective spin excitations since INS has the capability to probe spatial correlations of magnetic moments as well as their dynamical properties. In this section, the spin dynamics of $Na_3Co(CO_3)_2Cl$ is explored by means of INS as a function of both energy and momentum transfer over the reciprocal space.

Figure 12 shows a contour plot of the dynamic structure factor $S(Q,\omega)$ of $Na_3Co(CO_3)_2Cl$. The negative and the positive energy transfers correspond to the loss and the gain, respectively, of neutron energy in the scattering events. The red riff at around zero-energy transfer consists of an elastic incoherent-scattering component and nuclear Bragg reflections. As indicated by the white arrows in Fig. 12, the first seven nuclear Bragg peaks correspond to reflections (111) at 0.78 $Å^{-1}$, (022) at 1.27 $Å^{-1}$, (113) at 1.49 $Å^{-1}$, (222) at 1.55 $Å^{-1}$, (004) at 1.80 $Å^{-1}$, (133) at 1.96 $Å^{-1}$, and (224) at 2.20 $Å^{-1}$, consistent with the NPD of $Na_3Co(CO_3)_2Cl$. The magnetic intensity covers an energy-transfer range up to about 3 meV and reflects the overall energy scale of the magnetic exchange, which is in reasonable agreement with $|\Theta_{CW}| =$ 33.8 K as determined in the susceptibility measurements. At $T = 3.5$ K, magnetic scattering intensity is dominated by the

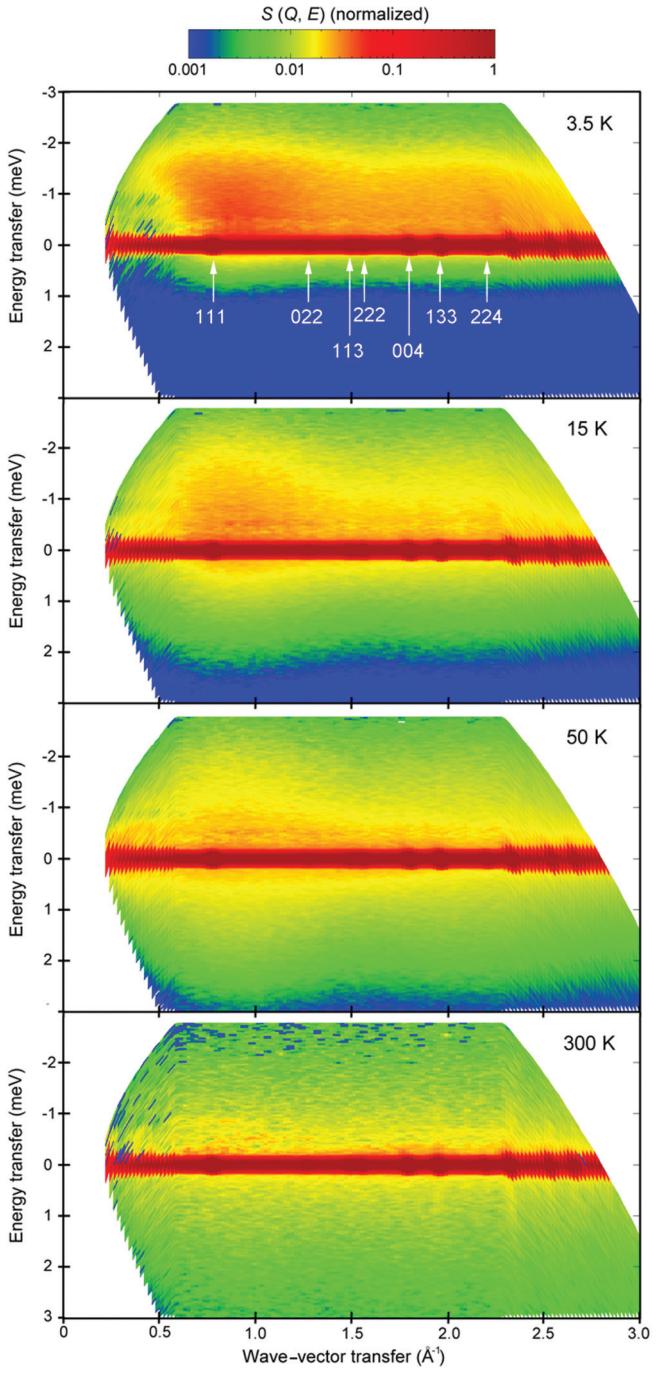

FIG. 12. (Color online) Contour plot of the dynamic structure factor $S(Q,\omega)$ of $Na_3Co(CO_3)_2Cl$ at 3.5, 15, 50, and 300 K. Magnetic intensity on the logarithmic scale is coded with colors from blue to red to indicate increasing intensities.

neutron energy-loss process. The Q dependence of magnetic scattering indicates a modulation around the magnetic form factor. A spin-wave-like profile centers at around 0.9 $Å^{-1}$, which is rather broad but still visible by comparing the difference in the low-Q regions in plots for 3.5 and 15 K. At 300 K (well above $|\Theta_{CW}| = 33.8$ K), quasielastic magnetic scattering for a purely paramagnetic state is expected.

The line shape and temperature dependence of the magnetic component is examined by considering the following general expression for the dynamic structure factor $S(Q,\omega,T)$, which is proportional to the imaginary part of the generalized susceptibility,[66]

$$S(Q,\omega,T) = \hbar\omega\left[1-\exp\left(-\hbar\omega/k_BT\right)\right]^{-1}\chi''(Q,\omega,T). \tag{11}$$

$[1-\exp(-\hbar\omega/k_BT)]^{-1}$ is the detailed balance factor representing the difference in the scattering function on the neutron

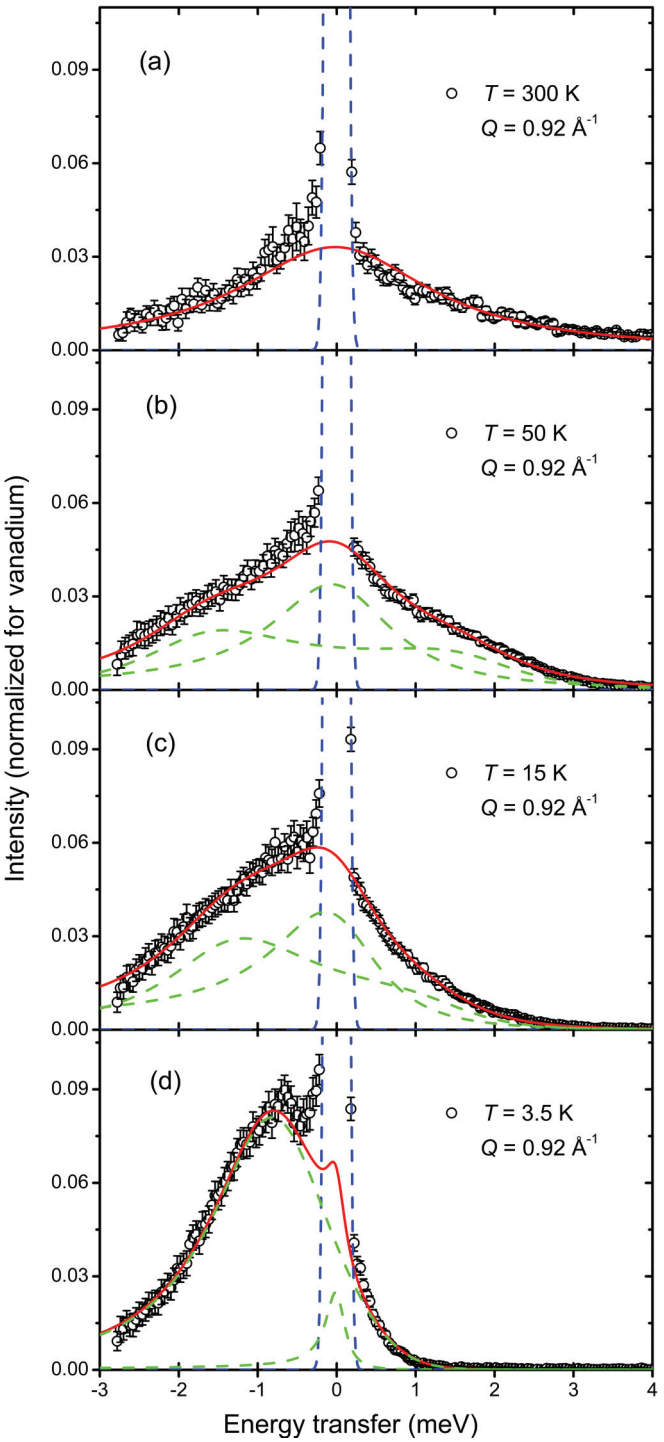

FIG. 13. (Color online) Dynamic structure factor $S(Q,\omega)$ of $Na_3Co(CO_3)_2Cl$ for constant wave-vector transfer $Q = 0.92$ $Å^{-1}$ at various temperatures.

energy gain and loss side due to the thermal population. $\chi''(Q,\omega,T)$ is taken as a Lorentzian-shaped quasielastic line with width Γ at sufficiently high temperatures,

$$\chi''(Q,\omega,T) = \chi_0(Q,T)\frac{\Gamma(Q,T)}{\omega^2+\Gamma^2(Q,T)}. \quad (12)$$

Figure 13 shows the cuts of $S(Q,\omega)$ for constant $Q = 0.92$ Å^{-1} at the investigated temperatures. The central elastic peak is fitted with a single Gaussian function (blue dashed line), whose width corresponds to the energy resolution of TOFTOF. The quasielastic component is fitted with a single Lorentzian function given by Eq. (12), multiplying a detailed balance factor. Upon cooling, collective magnetic excitations give rise to inelastic signals due to the increasing magnetic correlations. The low-T inelastic signals can be fitted with a damped harmonic oscillator (DHO) model multiplied by the detailed balance factor,[66–68]

$$S(Q,\omega) = \frac{A_{\mathrm{DHO}}\omega\Gamma_{\mathrm{DHO}}}{\left(\omega^2-\omega_{\mathrm{DHO}}^2\right)^2+(\omega\Gamma_{\mathrm{DHO}})^2}\frac{1}{1-e^{-\hbar\omega/k_{\mathrm{B}}T}}, \quad (13)$$

where A_{DHO} is the oscillator strength. The FWHM of the inelastic damped harmonic oscillator function is denoted as Γ_{DHO}, and the position of the peaks is $\pm\omega_{\mathrm{DHO}}$.

The quasielastic and inelastic components are shown by the green dashed lines in Fig. 13. The red lines in Fig. 13 represent the sum of quasielastic and inelastic components. At 300 K, the quasielastic intensity can be described by a single Lorentzian. No inelastic component is observed. Upon cooling the system to 50 K, which is above the modulus of the Curie-Weiss temperature but below the deviation temperature from Curie-Weiss law, a single Lorentzian cannot represent the data well. Additional inelastic components have to be involved to yield a good fit to the broad-hump-like feature at around ± 2 meV. But at 50 K, the quasielastic component still dominates the INS spectrum. As the temperature decreases to 15 K, the inelastic component increases significantly and becomes dominant. The linewidth of the quasielastic component decreases upon decreasing temperatures, and the spectral weight of the quasielastic component is transferred to the inelastic component of the collective magnetic excitations. At $T = 3.5$ K $< T_{\mathrm{g}}$, the quasielastic line shrinks into the elastic line within the instrumental resolution. The shrinking

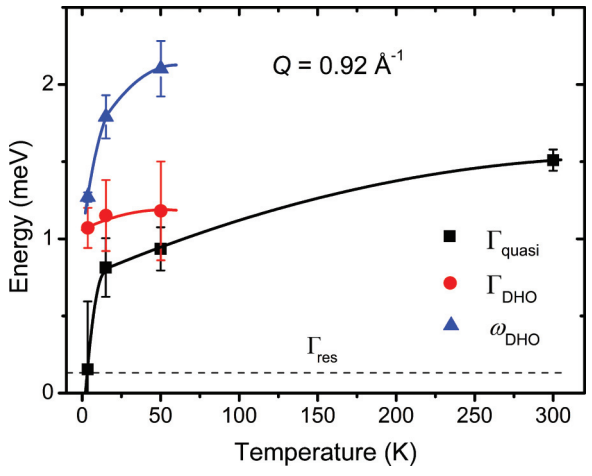

FIG. 14. (Color online) Temperature dependence of the linewidth and excitation energy of $Na_3Co(CO_3)_2Cl$ at $Q = 0.92$ Å^{-1}. The black squares represent the quasielastic linewidth Γ_{quasi}. The red circles and blue triangles show the linewidth Γ_{DHO} and the excitation energy ω_{DHO} of the inelastic components. The dashed line marks the instrumental energy resolution Γ_{res}. Black, red, and blue lines are guides to the eye.

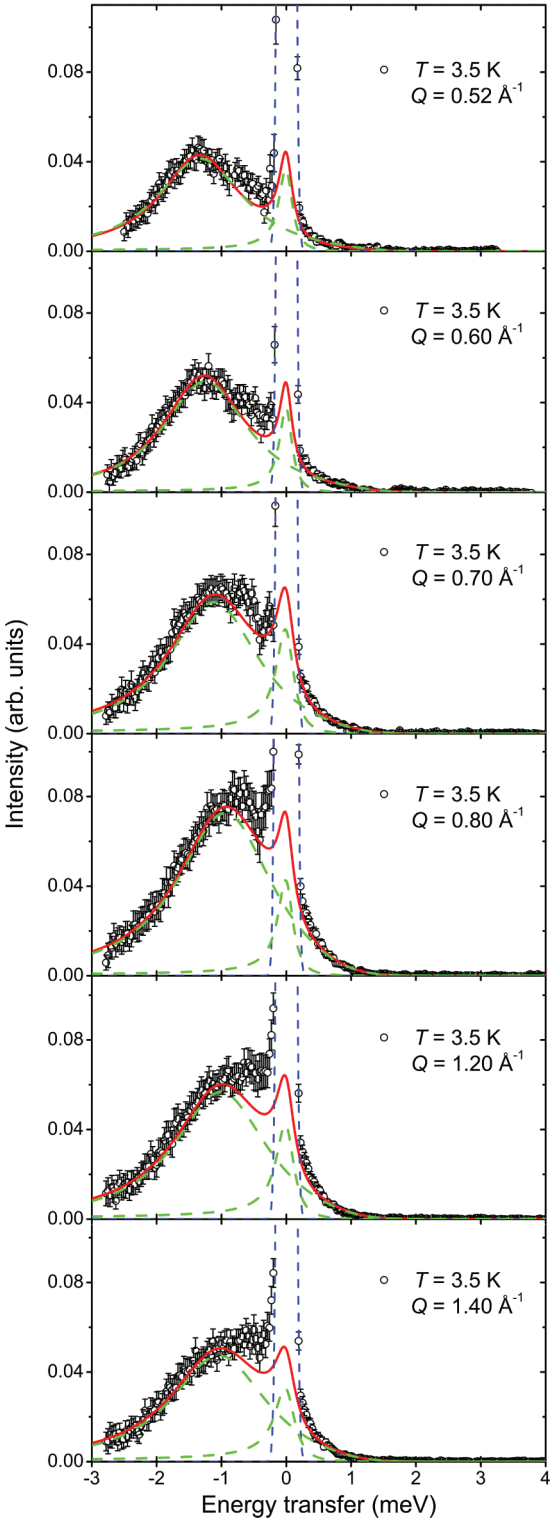

FIG. 15. (Color online) INS spectra for 3.5 K at various Q's along with the fit to the inelastic (red line) and the elastic (blue dashed line) components.

quasielastic component indicates a remarkable slowing down of the spin fluctuations. The magnetic scattering becomes basically inelastic with an excitation energy of about 1.3 meV at $Q = 0.92$ Å^{-1} at 3.5 K. The fitting results are summarized in Fig. 14, where Γ_{quasi} represents the FWHM of the quasielastic component.

As seen from the spectrum for $T = 3.5$ K, the magnetic scattering intensities seemingly emanated from the elastic line, although the inelastic feature is rather broad. The excitation energies for various Q's were investigated, and the corresponding quasielastic and inelastic components (green lines) were plotted in Fig. 15. The red line in Fig. 15 is the sum of quasielastic and inelastic components. The data in the range of $-0.7 < E < 0$ meV were excluded from the fitting consideration due to the high background in this energy region, resulting in the deviations between the data and the fitting results. The linewidths of the quasielastic components are comparable to the instrumental resolution. Clearly, the excitation energy of the inelastic component exhibits a Q dependence. The linewidth (Γ_{DHO}), the position (ω_{DHO}), and the integrated intensity (I_{DHO}) of the inelastic component are plotted in Fig. 16 as a function of Q. As shown in Fig. 16, the excitation energy of the inelastic component is about 1.54 meV at $Q = 0.52$ Å^{-1}. As Q increases, the excitation shifts to a lower energy and reaches a minimum at around $Q = 0.9$ Å^{-1}. If Q increases further from 0.9 Å^{-1}, the excitation shifts to a higher energy. Basically, the Q dependence of the excitation energy follows a spin-wave-like behavior. But besides this qualitative explanation for the Q dependence of the excitation energy, a reliable quantitative determination is difficult using the present data because the measured magnetic response is rather broad and is strongly affected by the secondary reflection of the neutron beam by the textured aluminum present in the neutron guide system before the sample.

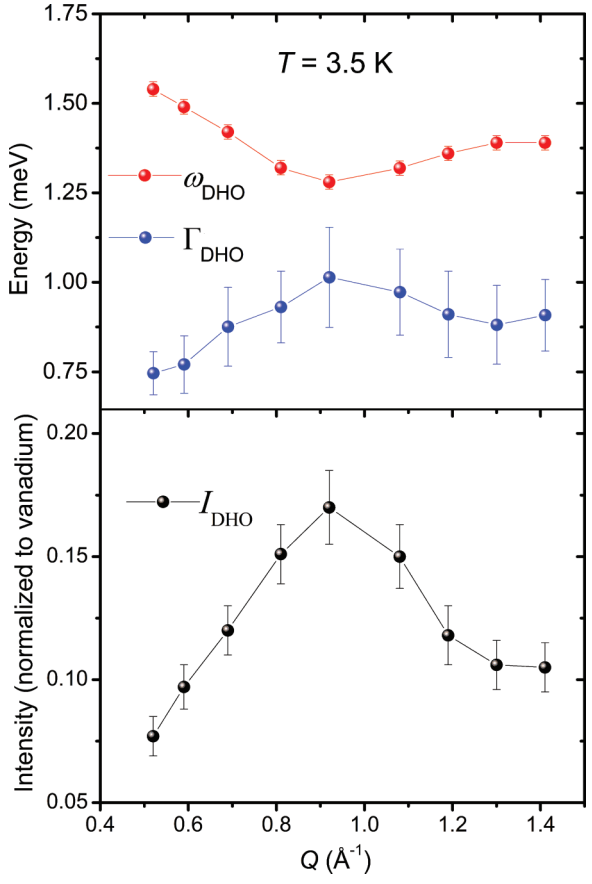

FIG. 16. (Color online) Q dependence of the linewidth (Γ_{DHO}), position (ω_{DHO}), and integrated intensity (I_{DHO}) of the inelastic components obtained by the fit to the INS spectrum for 3.5 K.

The inelastic neutron-scattering spectra of $Na_3Co(CO_3)_2Cl$, measured on TOFTOF, show clear collective magnetic excitations below 15 K. Especially, a spin-wave-like inelastic-scattering feature was observed at 3.5 K (below $T_g = 4.5$ K), which indicates that the freezing temperature T_g does not correspond to a complete spin-glass freezing as expected in canonical spin glasses.[26,27] But it should be noticed that, in Fig. 16, the minimum of the position of the inelastic component locates around $Q = 0.9$ Å^{-1}, inconsistent with the positions of the magnetic reflections observed in DNS measurements. This question will be explored through future inelastic neutron-scattering experiments on $Na_3Co(CO_3)_2Cl$ below 1.5 K.

IV. DISCUSSION

We have investigated a new spin-frustrated pyrochlore antiferromagnet $Na_3Co(CO_3)_2Cl$, which exhibits complicated magnetic behavior. At room temperature, the spins are paramagnetic. As the temperature decreases below 220 K, deviation from the Curie-Weiss law occurs. Spin correlations start to develop from, at least, 50 K, higher than $|\Theta_{CW}| \approx 33.8$ K. At 17 K, a long-range collective magnetic behavior happens, which exhibits a rather sharp feature in magnetic susceptibility and a small hump in specific heat. But the whole system does not display any long-range magnetic order detectable by neutron-scattering methods at 17 K. It seems that the spins are partially ordered at 17 K. As the temperature decreases further, the spin fluctuations slow down quickly. The spins experience a spin-glass-like freezing into the directions selected by local anisotropy at about 4.5 K, but this spin freezing is not complete in the sense that the spins may still be fluctuating with respect to the frozen directions. If the temperature keeps decreasing below the spin-glass-like freezing temperature, either an order-by-disorder mechanism, driven by the thermal and/or quantum fluctuations or structural distortion due to magnetocrystalline coupling, triggers a long-range magnetic order (or partial order) of this system.

It is an intriguing phenomenon that $Na_3Co(CO_3)_2Cl$ experiences a magnetic partial order at 17 K, a spin-glass-like transition at 4.5 K, and finally, a long-range magnetic order (or partial order) at 1.5 K. The origin of the magnetic partial order at 17 K is not clear. But a recent theoretical investigation by Chern *et al.* of a classical pyrochlore antiferromagnet may shed light on this magnetic partial order.[11] Their Monte Carlo simulations suggest a new partially ordered phase with collinear spins at finite temperatures in a classical Heisenberg pyrochlore antiferromagnet with a weak ferromagnetic next-nearest-neighbor interaction. In this intermediate partially ordered phase, the spins display collinear order within a thin {100} layer but no order across different layers,[11] which is similar to the magnetic behaviors of $Na_3Co(CO_3)_2Cl$ observed

at 17 K. A tentative explanation is given here that the system enters an intermediate partially ordered magnetic phase at 17 K. The nature of the spin-glass-like transition at 4.5 K is controversial. Although the present NPD measurements show that $Na_3Co(CO_3)_2Cl$ is chemically ordered within the experimental resolution, the subtle randomness of atomic bonds and/or the lattice distortion, triggered by magnetoelastic coupling, could be the source of disorder, serving as an ingredient of the spin-glass-like behavior in addition to the spin frustration.[38,39] The determination of the existence of local disorder in $Na_3Co(CO_3)_2Cl$ requires local probing methods, such as extended x-ray-absorption fine structure, nuclear magnetic resonance, or neutron pair distribution function analysis. The spin-glass-like behavior of $Na_3Co(CO_3)_2Cl$ at 4.5 K is different from that of canonical spin-glass systems in the sense that spins remain fluctuating below T_g instead of being frozen up, and moreover, a long-range magnetic order happens below T_g. A recent chirality scenario of the spin-glass ordering may provide an explanation for this controversy where the transition at T_g should actually correspond to a chiral-glass order.[69] Considering the local crystalline environment of Co^{2+} ions and some experimental facts presented above, $Na_3Co(CO_3)_2Cl$ behaves like a Heisenberg-type spin glass with weak anisotropy. Within the chirality-glass scenario, the transition at T_g is due to the freezing of the chirality rather than the spin itself. Therefore, the spins can remain dynamic below T_g. The Hall coefficient measurement[70] is needed to verify the chirality-glass scenario for the nonconventional spin-glass-like transition in $Na_3Co(CO_3)_2Cl$. For pyrochlore antiferromagnets with only nearest-neighbor interactions, there is a very high degree of frustration, and no long-range magnetic order is predicted. But long-range order may occur if a finite next-nearest-neighbor exchange interaction is considered.[9,11–13] For $Na_3Co(CO_3)_2Cl$, the weak ferromagnetic next-nearest-neighbor exchange interactions partially lift the vast degeneracy of the nearest-neighbor model and result in a magnetically ordered ground state. A mean-field approach to the magnetic ordering in pyrochlore antiferromagnets with ferromagnetic next-nearest-neighbor interactions predicted a ground state with incommensurate magnetic order,[12] whereas, a later Monte Carlo simulation on such a spin system suggested that the spins tend to order in a finite long-range order characterized by the commensurate spin order and remain largely fluctuating even in the ordered state.[13] A long-range magnetically ordered state of $Na_3Co(CO_3)_2Cl$ has clearly been indicated in our specific heat and polarized neutron-scattering measurements. But our experiments cannot identify whether the spins order completely in the ground state. A representation analysis of the magnetic reflections, obtained at 50 mK, suggest that $Na_3Co(CO_3)_2Cl$ exhibits a commensurate magnetic order with an all-in–all-out type spin arrangement. A full characterization of this long-range magnetic order requires samples with larger crystal sizes and more neutron-scattering experiments below 1.5 K.

V. CONCLUSION

In conclusion, the magnetism of spin-frustrated pyrochlore antiferromagnet $Na_3Co(CO_3)_2Cl$ has been investigated by means of various methods. The average crystal structure of $Na_3Co(CO_3)_2Cl$ has been determined and has been refined. The dc and ac magnetic susceptibility measurements provide strong evidence for a spin-glass-like transition at $T_g = 4.5$ K, which is in strong contrast to the conventional spin glasses because the spins of $Na_3Co(CO_3)_2Cl$ remain dynamic below T_g. An intermediate partially ordered phase and a long-range magnetic order (or partial order) have been observed at 17 and 1.5 K, respectively, qualitatively consistent with the theoretical predictions for pyrochlore antiferromagnets with weak ferromagnetic next-nearest-neighbor interactions. As a new model system of pyrochlore magnets, $Na_3Co(CO_3)_2Cl$ certainly deserves more experimental and theoretical investigations to understand the particular intermediate partially ordered state and the long-range ordering state as well as the nature of the spin-glass-like phase transition.

ACKNOWLEDGMENTS

The authors thank B. Schmitz and H. Schneider for their help with specific heat and diffuse neutron-scattering measurements. We also thank J. Voigt and W. Schweika for helpful discussions.

*fuzhendong@gmail.com
†zhengyanzhen@gmail.com
‡t.brueckel@fz-juelich.de

[1] P. W. Anderson, Mater. Res. Bull. **8**, 153 (1973).
[2] A. P. Ramirez, Annu. Rev. Mater. Sci. **24**, 453 (1994).
[3] R. Moessner and A. P. Ramirez, Phys. Today **59**, 24 (2006).
[4] J. S. Gardner, M. J. P. Gingras, and J. E. Greedan, Rev. Mod. Phys. **82**, 53 (2010).
[5] P. W. Anderson, Phys. Rev. **102**, 1008 (1956).
[6] J. Villain, Z. Phys. B **33**, 31 (1978).
[7] J. Villain *et al.*, J. Phys. (Paris) **41**, 1263 (1980).
[8] M. J. Harris, M. P. Zinkin, Z. Tun, B. M. Wanklyn, and I. P. Swainson, Phys. Rev. Lett. **73**, 189 (1994).
[9] N. P. Raju, M. Dion, M. J. P. Gingras, T. E. Mason, and J. E. Greedan, Phys. Rev. B **59**, 14489 (1999).
[10] M. Ito *et al.*, J. Phys. Soc. Jpn. **69**, 888 (2000).
[11] G.-W. Chern, R. Moessner, and O. Tchernyshyov, Phys. Rev. B **78**, 144418 (2008).
[12] J. N. Reimers, A. J. Berlinsky, and A.-C. Shi, Phys. Rev. B **43**, 865 (1991).
[13] D. Tsuneishi, M. Ioki, and H. Kawamura, J. Phys.: Condens. Matter **19**, 145273 (2007).
[14] J. E. Greedan, J. Mater. Chem. **11**, 37 (2001).
[15] J. S. Gardner, B. D. Gaulin, S.-H. Lee, C. Broholm, N. P. Raju, J. E. Greedan, Phys. Rev. Lett. **83**, 211 (1999).
[16] B. D. Gaulin, J. N. Reimers, T. E. Mason, J. E. Greedan, and Z. Tun, Phys. Rev. Lett. **69**, 3244 (1992).
[17] J. N. Reimers, J. E. Greedan, R. K. Kremer, E. Gmelin, and M. A. Subramanian, Phys. Rev. B **43**, 3387 (1991).
[18] B. Canals and C. Lacroix, Phys. Rev. Lett. **80**, 2933 (1998).

[19]J. S. Gardner *et al.*, Phys. Rev. Lett. **82**, 1012 (1999).
[20]Y. Machida, S. Nakatsuji, Y. Maeno, T. Tayama, T. Sakakibara, and S. Onoda, Phys. Rev. Lett. **98**, 057203 (2007).
[21]A. P. Ramirez *et al.*, Nature (London) **399**, 333 (1999).
[22]S. T. Bramwell and M. J. P. Gingras, Science **294**, 1495 (2001).
[23]J. E. Greedan, J. N. Reimers, C. V. Stager, and S. L. Penny, Phys. Rev. B **43**, 5682 (1991).
[24]M. J. P. Gingras, C. V. Stager, N. P. Raju, B. D. Gaulin, and J. E. Greedan, Phys. Rev. Lett. **78**, 947 (1997).
[25]N. P. Raju, E. Gmelin, and R. K. Kremer, Phys. Rev. B **46**, 5405 (1992).
[26]J. A. Mydosh, *Spin Glasses: An Experimental Introduction* (Taylor & Francis, London, 1993).
[27]K. Binder and A. P. Young, Rev. Mod. Phys. **58**, 801 (1986).
[28]M. J. P. Gingras *et al.*, J. Appl. Phys. **79**, 6170 (1996).
[29]E. F. Shender, V. B. Cherepanov, P. C. W. Holdsworth, and A. J. Berlinsky, Phys. Rev. Lett. **70**, 3812 (1993).
[30]J. R. L. de Almeida, J. Phys.: Condens. Matter **11**, L223 (1999).
[31]S. Sachdev, Phys. Rev. B **45**, 12377 (1992).
[32]T. Brückel *et al.*, Z. Phys. B: Condens. Matter **97**, 391 (1995).
[33]T. Brückel *et al.*, Phys. Lett. A **162**, 357 (1992).
[34]J. E. Greedan *et al.*, Solid State Commun. **59**, 895 (1986).
[35]J. N. Reimers, J. E. Greedan, and M. Sato, J. Solid State Chem. **72**, 390 (1988).
[36]C. H. Booth, J. S. Gardner, G. H. Kwei, R. H. Heffner, F. Bridges, and M. A. Subramanian, Phys. Rev. B **62**, R755 (2000).
[37]A. Keren and J. S. Gardner, Phys. Rev. Lett. **87**, 177201 (2001).
[38]J. E. Greedan, D. Gout, A. D. Lozano-Gorrin, S. Derahkshan, Th. Proffen, H.-J. Kim, E. Božin, and S. J. L. Billinge, Phys. Rev. B **79**, 014427 (2009).
[39]O. Ofer, A. Keren, J. S. Gardner, Y. Ren, and W. A. MacFarlane, Phys. Rev. B **82**, 092403 (2010).
[40]M. Hoelzel *et al.*, Neutron News **18**, 23 (2007).
[41]J. Rodríguez-Carvajal, Physica B **192**, 55 (1993).
[42]W. Schweika and P. Böni, Physica B **297**, 155 (2001).
[43]O. Schärpf and H. Capellmann, Phys. Status Solidi A **135**, 359 (1993).
[44]T. Unruh, J. Neuhaus, and W. Petry, Nucl. Instrum. Methods Phys. Res. A **580**, 1414 (2007).
[45]Y. Zheng, A. Ellern, and P. Kögerler, Acta Crystallogr., Sect. C: Cryst. Struct. Commun. C **67**, i56 (2011).
[46]A.-J. Dianoux and G. Lander, *Neutron Data Booklet* (Institut Laue-Langevin, Grenoble, 2003).
[47]D. C. Wallace, *Thermodynamics of Crystals* (Dover, New York, 1998).
[48]B. M. Bartlett, J. Am. Chem. Soc. **127**, 8985 (2005).
[49]D. Mehandjiev and E. Nikolova, Thermochim. Acta **23**, 117 (1978).
[50]M. Kurmoo, Philos. Trans. R. Soc. London, Ser. A **357**, 3041 (1999).
[51]J. de Almeida and D. Thouless, J. Phys. A **11**, 983 (1978).
[52]D. N. H. Nam, K. Jonason, P. Nordblad, N. V. Khiem, and N. X. Phuc, Phys. Rev. B **59**, 4189 (1999).
[53]A. P. Young and H. G. Katzgraber, Phys. Rev. Lett. **93**, 207203 (2004).
[54]E. A. Velásquez, J. Mazo-Zuluaga, J. Restrepo, and Ò. Iglesias, Phys. Rev. B **83**, 184432 (2011).
[55]S. Bedanta and W. Kleemann, J. Phys. D: Appl. Phys. **42**, 013001 (2009).
[56]P. C. Hohenberg and B. I. Halpcrin, Rev. Mod. Phys. **49**, 435 (1977).
[57]J. Souletie and J. L. Tholence, Phys. Rev. B **32**, 516 (1985).
[58]A. Tari, *The Specific Heat of Matter at Low Temperatures* (Imperial College Press, London, 2003).
[59]R. G. Scurlock and W. N. R. Stevens, Proc. Phys. Soc. **86**, 331 (1965).
[60]M. W. Klein and R. Brout, Phys. Rev. **132**, 2412 (1963).
[61]I. A. Blech and B. L. Averbach, Phys. **1**, 31 (1964).
[62]G. Ferey *et al.*, Rev. Chim. Miner. **23**, 474 (1986).
[63]H. Shinaoka, T. Miyake, and S. Ishibashi, Phys. Rev. Lett. **108**, 247204 (2012).
[64]K. Tomiyasu *et al.*, J. Phys. Soc. Jpn. **81**, 034709 (2012).
[65]X. Wan, A. M. Turner, A. Vishwanath, and S. Y. Savrasov, Phys. Rev. B **83**, 205101 (2011).
[66]A. Krimmel, H. Mutka, M. M. Koza, V. Tsurkan, and A. Loidl, Phys. Rev. B **79**, 134406 (2009).
[67]B. Fåk and B. Dorner, Physica B **234–236**, 1107 (1997).
[68]G. Shirane, S. M. Shapiro, and J. M. Tranquada, *Neutron Scattering with a Triple-Axis Spectrometer* (Cambridge University Press, Cambridge, U.K., 2002).
[69]H. Kawamura, J. Phys. Soc. Jpn. **79**, 011007 (2010).
[70]T. Taniguchi, K. Yamanaka, H. Sumioka, T. Yamazaki, Y. Tabata, and S. Kawarazaki, Phys. Rev. Lett. **93**, 246605 (2004).